ANALYSIS OF PACKAGING EFFECTS ON THE PERFORMANCE OF THE MICROFLOWN

J.W. van Honschoten, D.-R. Yntema, M. Dijkstra, V.-B. Svetovoy, R.-J. Wiegerink, M. Elwenspoek

DTIP of MEMS & MOEMS Stresa, Italy, 26-28 April 2006

ANALYSIS OF PACKAGING EFFECTS ON THE PERFORMANCE OF THE MICROFLOWN

J.W. van Honschoten, D.R. Yntema, M. Dijkstra, V.B. Svetovoy, R.J. Wiegerink, M. Elwenspoek

Transducers Technology Laboratory, MESA$^+$ Research Institute,
University of Twente, the Netherlands.

ABSTRACT

The packaging effects of an acoustic particle velocity sensor have been analysed both analytically and by means of finite volume simulations on fluid dynamics. The results are compared with acoustic experiments that show a large magnification of the output signal of the sensor due to the mounting inside a cylindrically shaped package. The influences of the package consist of a decrease of the output signal at frequencies below 1 Hz, whereas signals with frequencies above 10 Hz are amplified by a constant factor of approximately 3.5 (11 dB). The analysis leads to an improved insight into the effects of viscosity and fluid flow that play a role in flow sensing and opens the way for further optimisation of sensitivity and bandwidth of the sensor.

1. INTRODUCTION

The 'Microflown' is a micromachined acoustic sensor that measures the particle velocity instead of the sound pressure, the quantity that is measured by conventional microphones [1-6]. Originally a flow sensor [7], it has been optimised for sound measurements. The sensor consists of two or three thin platinum wires (length 1500 μm, spacing 240 μm) on a silicon nitride carrier, that are electrically heated to about 600 K (see fig. 1). The metal pattern acts as temperature sensor *and* as heater. When a particle velocity is present, the temperature distribution around the resistors is asymmetrically altered. The temperature difference, and therefore the resistance difference, between the sensor wires is proportional to the particle velocity associated with the sound wave.

For measurement purposes, the sensor is placed in a package: a 7 cm long cylindrical probe of 13 mm diameter with two small cylinders of about 5 mm diameter at its end, with the microflown in between (see fig. 2). These two tiny cylinders on top protect the fragile wires of the sensor while the holder contains the electrical connections. Moreover, this packaging of the sensor influences also the fluid flow. It improves its sensitivity by a factor 3.5, or approximately 11 dB. That observation raised the need for a detailed investigation of these packaging effects, in order to optimise the sensor performance further. In this paper, this investigation is achieved both by a numerical analysis using a finite-volume simulation program, and by a theoretical description of the flow profile around the two small cylinders of the package.

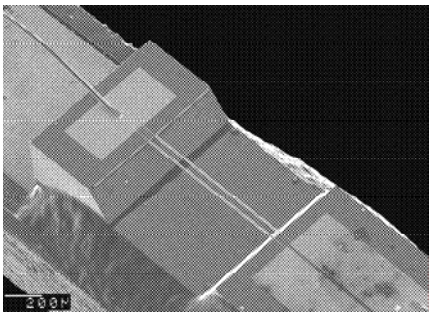

Fig. 1. SEM photograph of a two-wire type 'Microflown'.

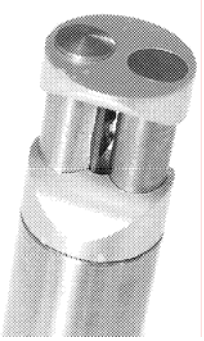

Fig. 2. The current probe, with the flow sensor packaged in between two tiny cylinders.

2. NUMERICAL SIMULATIONS

2.1. The approach

For numerical calculations on the complex structure of the package, we used a commercially available software

 ISBN: 2-916187-03-0

program, CFDRC, for fluid dynamical simulations [12, 13]. This software provides a variety of tools for the simulation and analysis of fluid flow. In our approach for the numerical simulation of the fluid behaviour around the sensor, three successive steps are to be distinguished.
The volume of interest (the solution space) is divided into discrete control volumes or cells.
The boundary conditions, the initial conditions and the equations to be solved at each cell are defined, as well as the numerical technique to solve the equations.
After the simulation, we extract the needed information from the large amount of data generated in the solution process.
The solution space was defined as a cylinder of approximately 8 cm radius and 15 cm height, in which the probe was positioned. A structured grid of tetrahedric and prismatic volume elements was designed in the fluid space around the probe. The number of cells amounted to about 70,000; in the middle, around the sensor, the cells were made very dense.
As a boundary condition, a plane propagating wave was imposed at the wall of the large outer cylinder. This wave was described by a varying fluid particle velocity of magnitude u_0 and radial frequency ω:

$$u(y,t) = u_0 \cos(\omega t - ky),$$

with k the wave number in the propagation direction y. The Navier–Stokes equations were solved at each fluid space element, together with the no-slip boundary condition on the probe surface and the assumption of a fully adiabatic process. Besides, a constant temperature and constant dynamic viscosity of respectively $T = 300$ K and $\nu = 1.5895 \cdot 10^{-5}$ m^2/s were assumed, an equilibrium fluid density of $\rho = 1.1614$ kg/m^3, and an equilibrium pressure of $p_0 = 1.0 \cdot 10^5$ Pa in the fluid around the probe. It must be mentioned that the temperature effects of the sensor, that causes a local temperature increase of the fluid due to the heated wires, have not been taken into account. Since this temperature effect is very localised and will therefore only slightly influence the fluid flow around it [4, 5], this assumption seems to be justified.
The numerical calculations were performed with a convergence criterion of 10^{-4}, using the SIMPLEC solution method, coupled with ideal gas law [11].

2.2. The fluid flow around the probe

In the different simulations, the frequency ω was varied between 0 and 10^4 rad/s, and the magnitude u_0 was chosen as $3 \cdot 10^{-5} < u_0 < 1 \cdot 10^{-3}$ m/s. Each simulation result

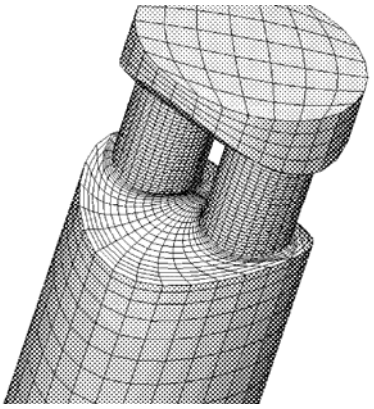

Fig. 3. A grid containing about 70 thousand cells was defined to model the probe geometry, very densely structured at the place of interest (the centre).

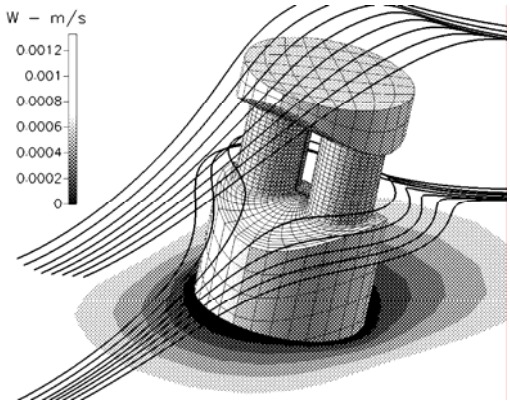

Fig. 4. Simulation result visualising both the streamlines and a contour plot of the particle velocity at $v_0 = 1$ mm/s; $f = 1$ Hz.

provided the magnitude and phase of the particle velocity and the pressure at each point in space, such that the streamline pattern in the fluid could also be investigated (fig. 4). It was observed that for the region of interest, $3 \cdot 10^{-5} < u_0 < 1 \cdot 10^{-3}$ m/s, all dynamics were linear in u_0, *i.e.* an increase of the amplitude of the imposed acoustic wave led to an entirely equal increase of all velocities and pressures in space.
We defined a number of points located in and around the probe to consider in particular:
Point A is located in between the two small cylinders (where the sensor is placed).
Point B is found at a distance of 8 cm in front of the probe (on the outer boundary where the acoustic wave is imposed).
Point C is located at 6.5 cm left from the centre.
Point D as a reference point for the phase of the wave, at 5 cm above A.

 ISBN: 2-916187-03-0

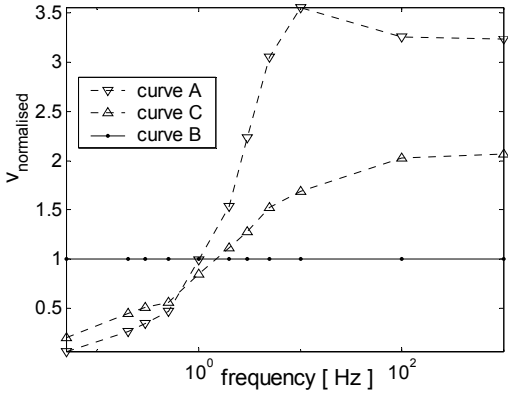

Fig. 5a. Amplitude of the particle velocity at different points in and around the probe. Point A: in between the two cylinders, B: at large distance in front of the probe, C: left from the probe, 6.5 mm from the center, D: 3 cm above A.

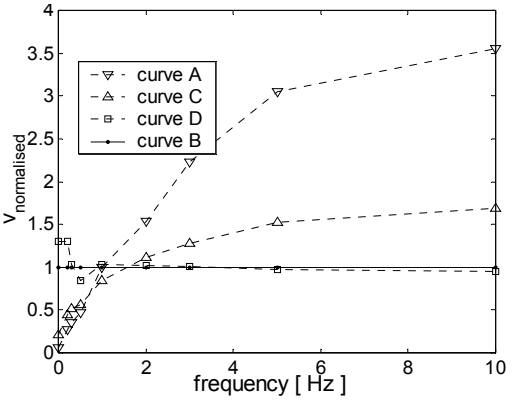

Fig. 5b. As fig. 5a, on a linear frequency scale.

When the frequency rises, the particle velocity (normalised to the value u_0 of the imposed wave) is seen to increase at both point A and C. One sees in fig. 5 that, especially at A, a large amplification of the particle velocity is attained. This magnification approaches a constant value of about 3.2 for frequencies above 10 Hz. However, for frequencies below 1 Hz, the normalised particle velocity at A is smaller than 1, and decreases to 0.1 at zero frequency. The same tendency is observed at C, a representative point for the region just next to the probe. The normalised signal increases from 0.2 at 0 Hz up to 1.7 at 10 Hz and then remains constant. The figures 5a and 5b show this behaviour on a linear and logarithmic frequency scale. At frequencies below the characteristic frequency of about $f_c = 1.5$ Hz, the (scaled) particle velocity amplitudes at A and C are lower than one, whereas for $f > f_c$, they increase.

3. THEORY

3.1. Introduction

To describe the flow behaviour around the sensor, the full Navier–Stokes equations for the three-dimensional geometry should be solved. Due to the complex geometry of the probe, an exact solution cannot be found. However, the region of interest is well approximated by two parallel long circular cylinders, so that the problem becomes actually two-dimensional. Oscillatory viscous flows around bodies of various shapes have been investigated in literature, see [8, 9]. We consider an incompressible viscous fluid with kinematic viscosity ν and density ρ in which two separated parallel cylinders are immersed. At infinity, the fluid oscillates harmonically, perpendicular to the plane containing their axes, with a velocity $u_0 \cos \omega t$. We show that this problem can be solved analytically and an explicit expression for the flow profile around the cylinders is found. Two regions of interest can be distinguished: a frequency range $\omega << \omega_c$, in which viscous effects are dominant and the viscous boundary layers around the cylinders become large, and a region $\omega >> \omega_c$, where the fluid behaviour approaches that of an ideal gas.
Besides, we show that for the ideal-gas case, a solution of the Navier–Stokes equations for this geometry is formed by vortices. In the entire description of the total solution, the contribution of vortices around the cylinders is largely responsible for the large magnitude of the particle velocity in between the cylinders at the location of the sensor; the observed 'package gain'.

3.2. Assumptions and problem definition

To find the flow profile in and around the probe, we have to solve the equations of motion of a viscous fluid, the Navier–Stokes equations, for the current geometry. To determine if the fluid in the case of propagating acoustic waves can be regarded as incompressible, we considered the conditions under which the assumption of incompressibility is justified. It was seen that for normal sound waves and frequencies well below 10 kHz, for the current geometry one can describe the gas as incompressible.
In their most general form the Navier–Stokes equations for an incompressible fluid then read

$$\frac{\partial \vec{v}}{\partial t} + (\vec{v} \cdot \vec{\nabla})\vec{v} = -\frac{1}{\rho}\vec{\nabla} p + \nu \nabla^2 \vec{v} \qquad (1.)$$

with $\vec{v}$ the (vectorial) velocity, p the pressure, ν the kinematic viscosity and ρ the fluid density.
Besides, the continuity equation has to be obeyed:

$$\frac{\partial \rho}{\partial t} + \vec{\nabla} \cdot (\rho \vec{v}) = 0 \qquad (2.)$$

For the three-dimensional geometry of the probe it is rather complicated to solve these equations analytically. But since the flow profile around the package in which the sensor is located is of main interest, we consider in particular the two cylindrical tubes of the package with the microflown in the middle.

Let us assume an infinite incompressible viscous fluid in which two parallel circular cylinders of radius R are immersed. The fluid oscillates in the direction perpendicular to the plane containing the axes of the cylinders with velocity $u_0 \cos \omega t$ at infinity where u_0 is the magnitude of the particle velocity and ω the radial frequency. The problem can be well described in a two-dimensional system of bipolar cylindrical coordinates (ξ,η), defined by the transformations

$$x = \frac{c \sinh \eta}{\cosh \eta - \cos \xi}, y = \frac{c \sin \xi}{\cosh \eta - \cos \xi}, \quad c > 0 \qquad (3.)$$

where x and y are the usual Cartesian coordinates, $0 \le \xi < 2\pi$ and $-\infty < \eta < \infty$ (see fig. 6).

The two cylinders are therefore defined by $\eta = \eta_1 > 0$ and $\eta = \eta_2 < 0$, where $R = c/|\sinh \eta_1| = c/|\sinh \eta_2|$. The fluid region is given by $\eta_2 < \eta < \eta_1$, $0 \le \xi < 2\pi$, while $\eta = \xi = 0$ at infinity.

The problem is scaled using the dimensionless parameters

$$\tau = \frac{\nu}{l^2} t, \qquad \mu = \frac{\omega l^2}{\nu} \qquad (4.)$$

where l represents a characteristic length, for example the cylinder radius.

The Navier–Stokes equations in the form (1.) are non-linear because of the second term on the left-hand side. This nonlinear problem has been analysed by Zapryanov et al. [8]. They used a perturbation theory in terms of asymptotic expansions in the inner and outer regions around the cylinders [8, 9].

3.3. Solution

For the current values in our problem, $u_0 \sim 2 \cdot 10^{-4}$ m/s, $l \sim 6 \cdot 10^{-3}$ m, $\nu \sim 1.5 \cdot 10^{-5}$ m^2/s, and $\omega > 60$ s^{-1}, the nonlinear convection term is of the order u_0^2/l and therefore relatively small compared with the other terms. Hence, we neglect the term $(\vec{v} \cdot \vec{\nabla})\vec{v}$ in the further approach. Moreover, we can assume $\mu >> 1$.

The Navier–Stokes equations, (1.), are often written in terms of the stream function Ψ, that in this coordinate system can be defined by

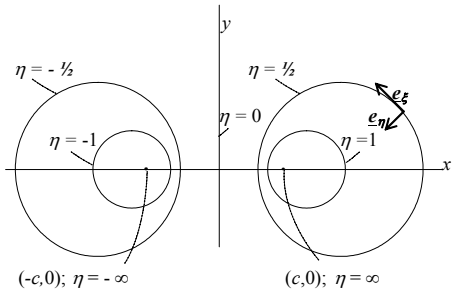

Fig. 6. Representation of the bipolar cylindrical coordinate system.

$$v_\xi = (ch\eta - \cos\xi)\frac{\partial \Psi}{\partial \eta}, \qquad v_\eta = -(ch\eta - \cos\xi)\frac{\partial \Psi}{\partial \xi} \qquad (5.)$$

We now have to solve the equations of motion for Ψ. For that purpose the fluid region around the two cylinders is divided in three regions: the two boundary layers adjacent to the cylinders, of thickness $\delta \sim \mu^{-1/2}$, and a region in between. The solution Ψ in the intermediate region forms the basis for a perturbation approach with a perturbation parameter μ, in the boundary layers. We deduced that one can write for the stream function in this region [10]:

$$\Psi(x,y) = \left(\frac{\exp 2(i \arctan(\frac{c}{y+ix}) - \eta_1)}{1 - \exp 2(i \arctan(\frac{c}{y+ix}) - \eta_1)} + \frac{\exp -2(i \arctan(\frac{c}{y-ix}) + \eta_1)}{1 - \exp -2(i \arctan(\frac{c}{y-ix}) - \eta_1)} - x \right) \exp(i\tau) \qquad (6.)$$

In the boundary layer adjacent to the right cylinder, a scaled variable ζ is defined:

$$\zeta = (\eta_1 - \eta)\sqrt{\mu} \qquad (7.)$$

The boundary layer extends from $\zeta = 0$ to $\zeta = 1$. The stream function in this region is Ψ_b, and μ is large but finite. The solution Ψ in the intermediate region forms the basis for a perturbation approach with a perturbation parameter μ, in the boundary layers. One finds then for the stream function in the boundary layer [10]:

$$\Psi_b(\xi,\zeta) = C_b \sinh(\sqrt{i}(\cosh\eta_1 - \cos\xi)\zeta) \qquad (8.)$$

with

$$C_b(\xi) = -\frac{1}{\sqrt{\mu}} \frac{\frac{\cosh\eta_1 \cos\xi - 1}{(\cosh\eta_1 - \cos\xi)^2} + 2\sum_{n=1}^{\infty} n \exp(-n\eta_1)\cos n\xi}{\sqrt{i}(\cosh\eta_1 - \cos\xi)\sinh(\sqrt{i}(\cosh\eta_1 - \cos\xi))} \qquad (9.)$$

 ISBN: 2-916187-03-0

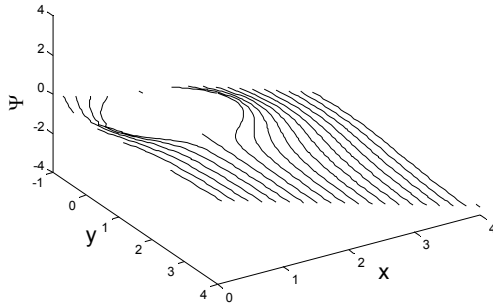

Fig. 7 Stream function Ψ. Contour lines of Ψ form streamlines in the flow.

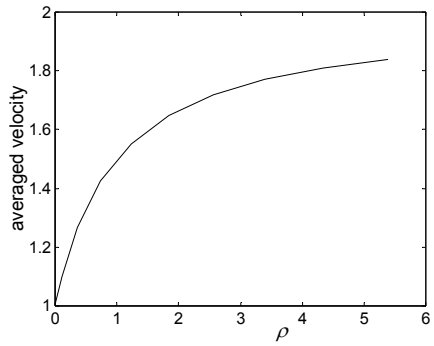

Fig. 8. The averaged normalised velocity as a function of the ratio of the cylinder radius and the spacing between the cylinders.
(ρ = cylinder radius/distance between cylinders).

In figure 7, the stream function according to eq. (6.) is visualised, for the half-infinite region $x > 0$ and a cylinder radius $R = \sinh^{-1}1$. ($c = \eta_1 = 1$). Contour lines of Ψ form the streamlines of the flow. With the expression obtained for the stream function, we can investigate the influence of the geometry on the velocity at the location of the sensor. Figure 8 shows the dependence of the flow velocity between the cylinders as a function of the ratio of the cylinder radius and the cylinder spacing. A good correspondence to the simulation results can be seen.

4. EXPERIMENTS

To determine the sensor sensitivity as a function of frequency, both a packaged and an unpackaged sensor were placed on a 'shaker' providing a broadband vibration. It was verified before that the response of the sensors, when both unpackaged, was identical. The ratio of the output signal of the packaged and unpackaged sensor was then measured using an audio analyser. Results are shown in fig. 9. The signal could be measured accurately down to frequencies of about 1 Hz.

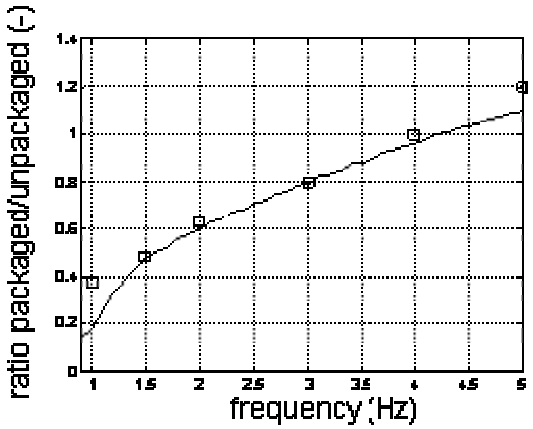

Fig. 9a. Ratio of the output signal of a packaged and an unpackaged sensor, as measured in a particle velocity measurement, for 0 < f < 5 Hz. The squares denote simulation results.

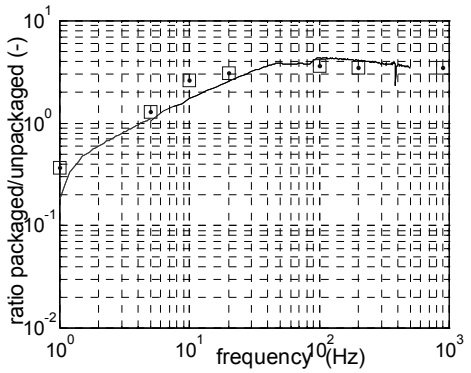

Fig. 9b. As fig. 9a, for the frequency range 1 < f < 500 Hz. The squares represent simulation results.

For $f < 4$ Hz, the ratio packaged / unpackaged output signal is smaller than 1, while for $f >> 4$ Hz, it approaches 3.2, remaining almost constant up to 10 kHz.

5. DISCUSSION

The Navier-Stokes equations were solved for the stream function Ψ, that provides all the information about the fluid velocity, in the different flow regions around the cylinders. The solution Ψ in the intermediate region formed the basis for a perturbation approach with a perturbation parameter μ, in the boundary layers.
Analysing the form of Ψ in eq. (6.), one can recognise three different elementary plane flow contributions [13, 14]: a contribution of the uniform flow, a 'doublet' flow or 'dipole' solution, and a so-called vortex flow. It is this vortex flow, which has an non-zero circulation along a contour around each of the cylinders, that is mainly responsible for the large magnification of the velocity in

 ISBN: 2-916187-03-0

between the cylinders. In between the two cylinders, the contributions of the two vortices around the two cylinders are of equal sign and therefore add.
This non-zero circulation along a contour around a cylinder is also observed in the numerical simulations.
Since the frequency parameter $\mu = \omega l^2/\nu$ is proportional to the frequency ω, the situation $\mu \to \infty$ describes the ideal fluid limit, and we are left with the solution for Ψ in the intermediate region; the boundary layer thickness decreases to zero. For μ small, say $\mu \sim 1$ (a low frequency, small characteristic length or high viscosity), the perturbation approach used cannot be applied. In this frequency range, the numerical simulations supplement the theoretic analysis. One can determine a certain characteristic frequency at which the boundary layers extend over all space between the cylinders. For the current geometry this frequency is approximately $f_c \approx 1.5$ Hz. This distinction between low and high frequencies is important for the acoustic measurement purposes of the microflown. The aim of the sensor is to measure frequencies in the acoustic range (from 20 Hz to 10 kHz) while lower frequencies are preferably suppressed. Experiments show that the current geometry of the probe magnifies signals higher than, and attenuates signals lower than, $f = 4$ Hz (which is in the same order of magnitude as f_c).

6. CONCLUSIONS

We have analysed the effects of the package of the microflown on the velocity profile around the flow sensor. Numerical simulations show a large magnification of the particle velocity in between the two small cylinders of the package where the sensor is mounted, for frequencies above 4 Hz. The magnification increases up to approximately 3.2 at high frequencies (10 Hz-10 kHz) and then remains constant. An analytic expression for the flow profile was also deduced, that explains adequately the package gain at high frequencies. The existence of vortices in the fluid flow is mainly responsible for this magnification. For low frequencies, viscous effects dominate and signals are attenuated. This is important for acoustic measurement applications, in which low frequency noise should be suppressed (to prevent overburding of the amplifier) and higher frequencies be amplified. We found a good correspondence between simulations, theory and experiments. This opens the way for further optimisation of the package geometry.

7. ACKNOWLEDGEMENT

This research was funded by the Dutch Technology Foundation (STW).

8. REFERENCES

[1] H-E. de Bree et al., The Microflown: a novel device measuring acoustical flows, *Sensors and Actuators A* 54 (1996), 552-557.
[2] www.microflown.com.
[3] W.F. Druyvesteyn et al., A new sound intensity probe; comparison to the Bruel and Kjaer p-p probe, *Proc.104th AES Convention* (1998)
[4] V.B. Svetovoy, I.A. Winter, Model of the Microflown microphone, *Sensors and Actuators* 86 (2000), 171-181.
[5] J.W. van Honschoten et al., Analytic model of a two-wire thermal sensor for flow and sound measurements, *Journal of Micromech. Microeng.*14 (2004) 1468-1477.
[6] J.W. van Honschoten et al., Optimisation of a two-wire thermal sensor for flow and sound measurements, *Proc. MEMS 2001.*
[7] T.S.J. Lammerink et al., Micro Liquid Flow Sensor, *Sensors and Actuators A*, (1993), 37-38, 45-50.
[8] Z. Zapryanov, Zh. Kozhoukharova, A. Iordanova, On the hydrodynamic interaction of two circular cylinders oscillating in a viscous fluid, *J. of Applied Math. and Phys*., (1988) vol. 39.
[9] C.Y. Wang, On high-frequency oscillatory flows, *J. Fluid Mech*., (1968), vol. 32, part 1, p 55-68.
[10] J.W. van Honschoten et al., 'Analysis of packaging effects on the performance of the microflown', to be published.
[11] CFD Research Corporation, technologies for engineering simulations (Huntsville, Alabama, USA), www.cfdrc.com.
[12] H. Versteeg, W. Malalasekra, 'An Introduction to Computational Fluid Dynamics: The Finite Volume Method Approach', 1996.
[13] L.D. Landau, E.M. Lifschitz, 'Course of Theoretical Physics', vol. 6, Fluid Mechanics, 2nd ed. 2003.
[14] R. W. Fox, A.T. McDonald, 'Introduction to Fluid Mechanics', third edition, 1985.

 ISBN: 2-916187-03-0